Self-sustained photothermal oscillations in high-finesse Fabry-Perot microcavities

Kumarasiri Konthasinghe, Juan Gomez Velez, Adam J. Hopkins, Manoj Peiris, Luisa T. M. Profeta, Yamil Nieves, and Andreas Muller

Phys. Rev. A **95**, 013826 — Published 18 January 2017

DOI: 10.1103/PhysRevA.95.013826

Self-sustained photothermal oscillations in high-finesse Fabry-Perot microcavities

Kumarasiri Konthasinghe,[1] Juan Gomez Velez,[1] Adam J. Hopkins,[2,*] Manoj Peiris,[1] Luisa T. M. Profeta,[2] Yamil Nieves,[1] and Andreas Muller[1,†]

[1] *Dept. of Physics, University of South Florida, Tampa, FL 33620*
[2] *Alakai Defense Systems, Largo, FL 33777*

We report the experimental investigation of a regime of microscopic Fabry-Perot resonators in which competing light-induced forces—photothermal expansion and photothermal refraction—acting oppositely and on different timescales lead to self-sustained persistent oscillations. Previously concealed as ordinary thermo-optic bistability—a common feature in low-loss resonator physics—these dynamics are visible as fast pulsations in cavity transmission/reflection measurements at sufficiently high time resolution. Their underlying mathematical description is shared by many slow-fast phenomena in chemistry, biology and neuroscience. Our observations are relevant in particular to microcavity applications in atom optics and cavity quantum electrodynamics, even in nominally rigid structures that have not undergone lithography.

I. INTRODUCTION

Due to their ability to recirculate light at a resonant frequency with ultralow loss [1], high-finesse optical resonators have become an indispensable tool in diverse research areas such as optomechanics [2–4], gravitational wave detection [5], atom optics [6], and solid-state cavity quantum electrodynamics [7]. The build-up of photons inside an optical resonator can substantially enhance light-matter interactions at a microscopic scale, thus providing a multitude of practical applications, for example in trace gas detection [8, 9]. In addition, high-finesse optical resonators offer unsurpassed displacement sensitivity, routinely on the picometer scale and below $10^{-19}\mathrm{m}/\sqrt{\mathrm{Hz}}$ in the recent milestone laser interferometer gravitational-wave observatory (LIGO) measurements [5]. Because of these properties, the power circulating within an optical resonator is uniquely sensitive to a variety of forces. In particular, it is sensitive to those forces which it itself induces as it reflects off the resonator's boundaries.

Even for boundary surfaces with near-unity reflectivity and in the absence of electronic material resonances, a multitude of interactions can arise, including the optical Kerr effect causing a nonlinear refractive index, radiation pressure due to photon momentum conservation, electrostriction associated with light-induced lattice deformation, refractive index change due to heating, and thermal expansion due to heating, amongst others. The magnitude and polarity of these effects depends strongly on the type of resonator and its morphology.

In monolithic whispering gallery resonators, e.g., silica toroids or microspheres, radiation pressure often dominates all other effects, making them popular for cavity optomechanics experiments [2]. Coincidentally, in such resonators, the aforementioned processes all cause an increase in the effective cavity length when the intracavity power increases [10].

In contrast, the effective cavity length of a Fabry-Perot resonator can either increase or decrease with intracavity power depending on the interaction. For instance, photothermal expansion causes a *decrease* in the cavity length, but photothermal refraction, i.e., the increase of the refractive index of the coating due to heating, causes an *increase* in the effective cavity length [11]. Moreover, radiation pressure always causes an increase in the length of a Fabry-Perot cavity, as does the Kerr effect. As a result, when photothermal expansion is the dominant force decreasing the cavity length, a Fabry-Perot cavity can sustain a regime in which photothermal expansion competes with either radiation pressure or photothermal refraction, acting on different timescales.

We explore here the nonlinear dynamics that result from this competition for the case of a *microscopic* Fabry-Perot resonator with dimensions of ∼10 μm, constructed with mirrors laser-machined on bulk substrates. Marin and Marino *et al.* have extensively investigated theoretically and experimentally the slow-fast "canard" dynamics exhibited by *macroscopic* resonators when one of the mirrors is mechanically compliant with well-defined eigenmodes [12, 13]. We find that even for resonators not purposefully designed to couple to specific mechanical modes, slow-fast dynamics take place. The most striking observation associated with the slow-fast dynamics are persistent high-amplitude oscillations of intracavity power at >1 MHz frequency, visible once input powers reach ∼ 10 mW for a cavity finesse $\gtrsim$ 30 000. A theoretical analysis establishes that the primary origin of these dynamics is the competition of photothermal expansion and photothermal refraction on timescales of order 10 μs and 0.1 μs, respectively.

II. EXPERIMENTS

The type of cavity investigated in this work is based on low-loss SiO_2/Ta_2O_5 dielectric mirrors (reflectivity $R \gtrsim$ 99.99%) in close proximity to each other (cavity length

*Current address: Metrohm USA, Inc., Riverview, FL 33578
†Electronic address: mullera@usf.edu

$L \lesssim 10$ μm). For such a small mirror separation, the resulting cavity photon lifetime is only $\tau_c \approx \frac{L/c}{1-R}$ ∼1 ns, where c is the speed of light. This time is much smaller than the cavity photon lifetime in macroscopic Fabry-Perot resonators commonly under study, for which $L \sim 10$ cm is typical [11]. Since displacement sensitivity is independent of cavity length, the microscopic cavity length enables one to reach dynamics that are not limited by cavity photon build-up or decay.

The specific cavity probed here consisted of one planar mirror mounted opposite another mirror having a concave surface indentation created by CO_2 laser ablation (radius of curvature ROC ≈ 50 μm) [6, 14, 15]. The ultrasmooth surface reflown by the CO_2 laser leads to low absorption and scatter losses so that the finesse, $\mathcal{F} \approx \pi/(1-R)$, is near 60 000 for the combination of mirrors employed here. A set of piezoelectric transducers (PZTs) controlled the mirror separation at a coarse and fine level independently to minimize the influence of electric noise. The cavity transmission and reflection were recorded with a fast photodetector (bandwidth >100 MHz) while the light from a diode laser (linewidth <5 MHz) coupled to a TEM_{00} mode of the cavity through a single achromatic lens.

Figure 1 shows the recorded cavity transmission, for a fixed laser wavelength of $\lambda \approx 922$ nm, as the cavity length was varied using a triangular waveform applied to the PZTs. The left part of Fig. 1(a) shows transmission during the "up-ramp" (increase in cavity length) while the right shows the corresponding data during the "down-ramp" (decrease in cavity length), for various laser input powers, $P_{\rm in}$, as indicated. Fig. 1(b) shows a zoomed view of cavity transmission during the down ramp.

As can be seen, there is a significant difference between the recorded transmission peaks for up and down ramps once the input power exceeds ∼1 mW. A bistable behavior of this kind is very common in all types of high-finesse resonators [10, 15–17]: the small residual photon energy lost in the mirrors causes heating, which in turn leads to a shift in the cavity resonance frequency (typically via thermal expansion). Depending from which side the resonance is approached, the approach is either accelerated or decelerated by this photothermal effect, thus giving rise to seemingly broadened or narrowed lineshapes.

However, in the data of Fig. 1(a), the observed transmission lineshapes also have a fast substructure with sig-

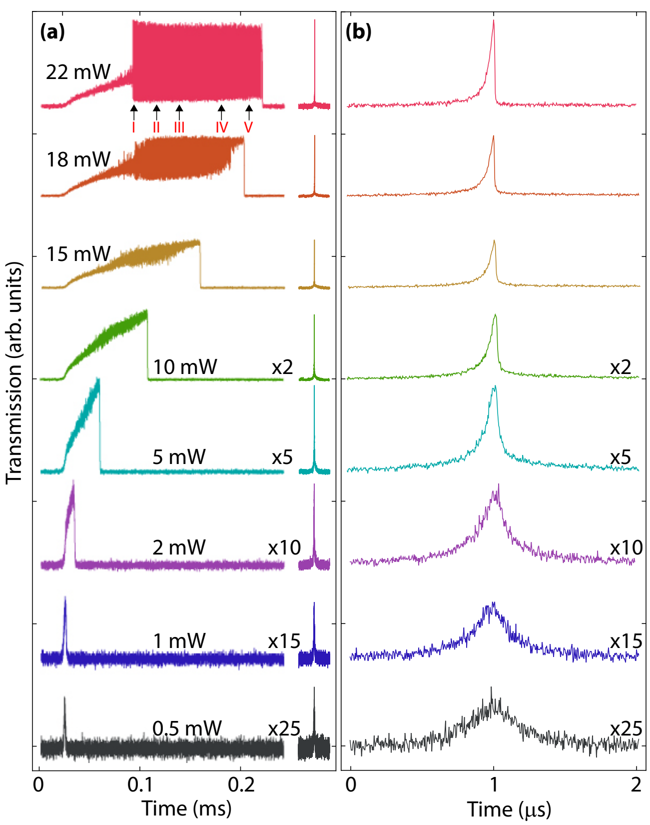

FIG. 1: (a) Transmission of microcavity as its length is being varied at a rate of 8.8 pm/μs by PZTs, for a set of laser input powers, $P_{\rm in}$. In the left (right) traces the length is being increased (decreased). (b) Zoomed view into the right traces of Fig. 1(a).

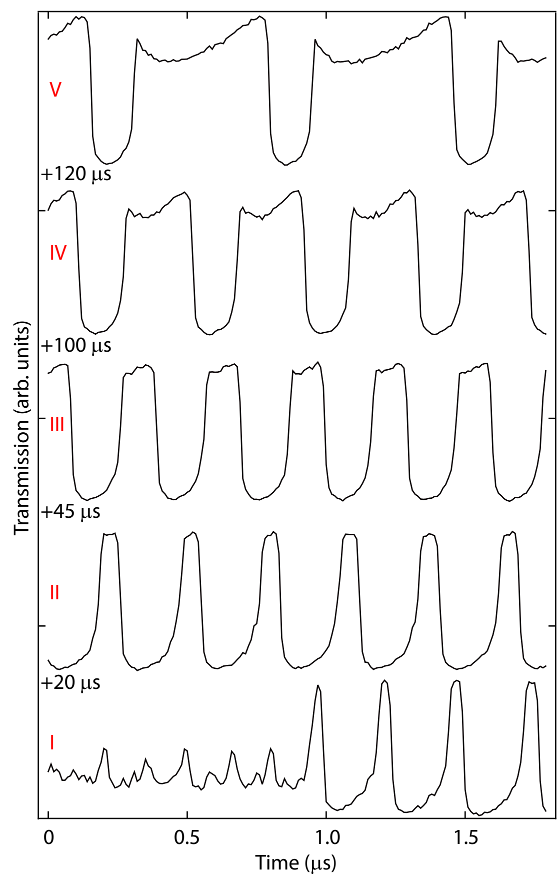

FIG. 2: Zoomed view of the oscillatory regions of the $P_{\rm in}$ = 22 mW "up-ramp" data of Fig. 1(a). The Roman numerals indicate the starting time of each trace (offset vertically for clarity) in relation to the representation in Fig. 1(a).

nificant amplitude once $P_{\rm in} \gtrsim 10$ mW. A zoomed view of this substructure is shown in Fig. 2 for various time windows as indicated on the up-ramp data of Fig. 1(a) at $P_{\rm in} = 22$ mW. This substructure is very different from that observed in whispering gallery optomechanical microresonators [2, 18], where it is directly associated with a specific mechanical oscillation frequency. Here, an evolution from high-frequency harmonic oscillations to lower frequency pulsations is seen when the peak transmission is approached.

III. ANALYSIS

To understand how such pulsations can emerge in this simple experiment, it is helpful to estimate the magnitude and timescale associated with various effects as they cause a shift of the cavity resonance frequency. Such estimates require a knowledge of the waist of the cavity mode (on the planar mirror), w_0, and known material parameters such as density, ρ, thermal conductivity, κ, specific heat, s, and coefficient of thermal expansion, $C_{\rm ex}$, of the mirrors.

From the experimentally measured cavity free spectral range of FSR ≈ 23 THz, we obtain the cavity length $L \approx c/(2\times\text{FSR}) \approx 6.5$ µm which can then be used to estimate the mode spot size as $w_0 = \sqrt{\lambda((\text{ROC}-L)L)^{1/2}/\pi} \approx 2.2$ µm [19]. From the low power data of Fig. 1(a) we can further obtain the full width at half maximum (FWHM) in displacement, $d_{\rm FWHM}$, associated with the cavity resonance. Writing the Lorentzian resonance profile as $\mathcal{L}(x) = 1/(1+(4\mathcal{F}x/\lambda)^2)$, we extract $d_{\rm FWHM} = \lambda/2\mathcal{F} \approx$ 9 pm. Finally, we estimate that mirror absorption is $\mathcal{A} \approx$ 10 ppm (parts per million) and that the power circulating in the cavity is $P_{\rm circ} = \alpha P_{\rm in}\mathcal{L}(x)$, with $\alpha \approx 5000$ a dimensionless proportionality constant accounting for imperfect mode/impedance matching and losses. With these values, the highest average circulating intensity in this experiment was $I_{\rm circ} \approx 700$ MW/cm^2.

A. Nonlinear index effects

Due to this relatively high circulating intensity it is reasonable to expect an influence of the optical Kerr effect. However, assuming the nonlinear index of refraction of the mirror coating is near that of fused silica, i.e., $n_2 \approx 3(10)^{-16}$ cm^2/W [20], one finds a maximal change in refractive index of $\Delta n = n_2 I_{\rm circ} \approx 2(10)^{-7}$. In addition, electrostriction, which may also be viewed as an effective nonlinear index effect with $n_2^{(str)} \approx 0.6(10)^{-16}$ cm^2/W [21], provides an even smaller contribution of about $\Delta n = n_2^{(str)} I_{\rm circ} \approx 4(10)^{-8}$. Using the transfer matrix method to calculate the cavity resonance length for two Bragg mirrors of the kind employed here, it is found that the change in the cavity resonance length due to a change in the index of refraction of the coating material is given approximately by $\Delta L/\Delta n \approx 1.5$ µm for $\Delta n \ll 1$. Therefore the maximal change in cavity length due to the combined influence of the optical Kerr effect and electrostriction is $\Delta L \approx 0.3$ pm, and can thus be safely ignored because it is much smaller than $d_{\rm FWHM}$.

B. Radiation pressure

The force due to radiation pressure acting on each mirror is given by $F_{\rm rp} = 2P_{\rm circ}/c$, and is thus as high as ≈ 1 µN in our experiment. We have performed finite element simulations of the resulting indentation under stationary conditions assuming the contact area of the force is πw_0^2, and the material is fused silica, with Young's modulus of 73 GPa and Poisson's ratio of 0.17. The resulting maximal indentation for each mirror was found to be ≈ 1.5 pm, so that the total cavity length change due to radiation pressure was maximally ≈ 3 pm. This suggests that radiation pressure only plays a secondary role in our measurements, because a displacement of 3 pm from peak resonance would only reduce transmission by less than half its maximum value, contrary to observations in Fig. 2. We note that non-stationary indentations with larger amplitudes, i.e, elastic waves, may be generated by the radiation pressure force. In fact, in previous work on cavities of lower finesse radiation pressure effects have been detected [22]. In addition, direct measurements of the amplitude of elastic waves induced by the reflection of a laser off a mirror with displacements of order 10 pm have been reported for a lower laser fluence than in the present experiment [23]. Radiation pressure effects have also been measured in mechanically compliant cavities based on mirrors at the tip of optical fibers [24]. More work is therefore needed to fully understand the effect of radiation pressure for the microcavities based on bulk substrates investigated here.

C. Thermal effects

By far the dominant light-induced cavity resonance shifts occur in our system because of residual absorption in the mirrors causing localized heating. An increased temperature of the mirrors causes two competing processes: (i) photothermal expansion of the mirror coating/substrate which *decreases* the cavity length, and (ii) photothermal refraction, i.e., an increase in the index of refraction of the coating due to heating which *increases* the effective cavity length. The timescale for these two processes differs significantly. Since the cavity field decays sharply inside the reflective coating (penetration depth < 1 µm), heat is deposited primarily near the surface and thus the temperature rises faster there than deeper in the mirror coating. The rapidly heated surface layers of the coating thus experience "fast" photothermal refraction, while the deeper layers experience "slow" photothermal expansion.

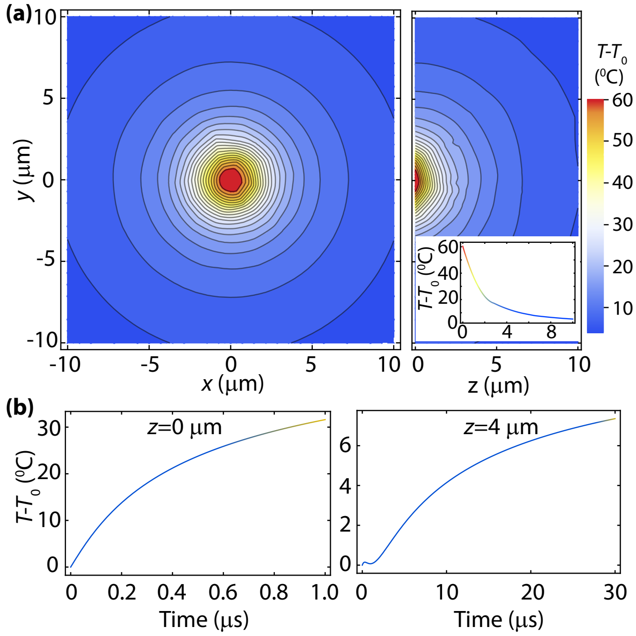

FIG. 3: (a) Contour plot of the stationary temperature ($t \to \infty$) on the mirror surface (left) and on the x=0 cross-sectional plane (right), obtained from a numerical solution of the heat diffusion equation for $P_{\rm circ}$ = 100 W. The inset shows the temperature along the z-axis. (b) On-axis temperature as a function of time at the surface (left) and 4 µm beneath the surface (right).

In order to estimate the magnitude and response time associated with these two processes, we have numerically solved the heat diffusion equation

$$\nabla^2 T(x,y,z,t) - \frac{s\rho}{\kappa}\frac{\partial T(x,y,z,t)}{\partial t} = 0, \tag{1}$$

where $T(x,y,z,t)$ denotes temperature. The mirror under consideration in our model is cylindrical with thickness d = 1 mm and diameter D = 4 mm. At its center, the mirror's front surface is experiencing a constant flux,

$$\vec{n}\cdot\nabla T(x,y,0,t) = -\frac{P_{\rm circ}\mathcal{A}}{\kappa\pi w_0^2} e^{-2\frac{x^2+y^2}{w_0^2}}, \tag{2}$$

where $\vec{n}$ is the outward-facing unit normal to the surface, while the back surface is maintained at constant temperature, $T(x,y,d,t) = T_0$. Fig. 3 depicts the results of the simulation, specifically the steady-state temperature distribution, $T(t\to\infty) - T_0$, [Fig. 3(a)] and temperature rise, $T(t) - T_0$, as a function of time at the surface ($z = 0$), and deeper inside the coating (z = 4 µm) [Fig. 3(b)], for $P_{\rm circ}$ = 100 W.

Fig. 3(a) shows that the temperature increase is localized to a region with a lateral extent of approximately w_0 and a longitudinal depth of approximately 4 µm, or about the thickness of the coating. The highest steady-state temperature, $T_{\rm max} \approx 60^{\rm o}$C, is reached on-axis at the surface. Fig. 3(b) reveals that within 0.2 µs the temperature at the surface has risen (nearly linearly) by about 13$^{\rm o}$C, and only changes slowly after a few microseconds have elapsed. By contrast, the temperature 4 µm inside the coating takes about 5 µs to change by the same proportion. Since the majority of thermal expansion is contributed by material up to a depth of around 4 µm [inset of Fig. 3(a)] we conclude that the timescale of photothermal expansion, τ_s, and that of photothermal refraction, τ_f, differ by about a factor of $\frac{\tau_s}{\tau_f} \approx \frac{5\mu\text{s}}{0.2\mu\text{s}} = 30$ for our particular experimental configuration.

The simulation of Fig. 3 also allows us to calculate power-dependent cavity resonance shifts for the two processes. For photothermal expansion we obtain a coefficient, B_s, computed as in Ref. [11], as

$$\begin{aligned} B_s &= -2\frac{C_{\rm ex}}{P_{\rm circ}\mathcal{A}}\int_0^\infty \Big(T(0,0,z',t\to\infty) - T_0\Big)dz' \\ &\approx -18 \text{ pm/W}, \end{aligned} \tag{3}$$

where the factor of 2 accounts for the fact that each mirror provides an (approximately) equal contribution and the minus sign indicates that photothermal expansion reduces the cavity length. The effective coefficient of thermal expansion of the coating, $C_{\rm ex}$ = $3.2(10)^{-6}/^{\rm o}$C, was obtained from the known expansion coefficients $(\Delta L/\Delta T)_{\rm SiO_2} \approx 6(10)^{-7}/^{\rm o}$C and $(\Delta L/\Delta T)_{\rm Ta_2O_5} \approx 5(10)^{-6}/^{\rm o}$C [25]. Furthermore, we can estimate the photothermal refractive cavity resonance shift in the form of a coefficient, B_f, calculated as

$$\begin{aligned} B_f &= +\Big(\frac{\Delta L}{\Delta T}\Big)\frac{\delta T}{P_{\rm circ}\mathcal{A}} \\ &\approx +1.1 \text{ pm/W}. \end{aligned} \tag{4}$$

For this estimate the transfer matrix method was used to calculate the change in cavity resonance length for a given change in temperature, found to be $\frac{\Delta L}{\Delta T} \approx 8.5$ pm/$^{\rm o}$C, via the known temperature dependence of the refractive indices of the coating layers. The latter have been experimentally measured as $(\Delta n/n\Delta T)_{\rm SiO_2} \approx 6$ ppm/$^{\rm o}$C and $(\Delta n/n\Delta T)_{\rm Ta_2O_5} \approx 1.1$ ppm/$^{\rm o}$C [26, 27]. Here the characteristic temperature change used in the calculation was $\delta T = 13^{\rm o}$C which has the associated timescale of τ_f = 0.2 µs [Fig. 3(b)].

IV. SLOW-FAST DYNAMICS MODEL

In order to model the dynamics generated by the interplay of photothermal expansion and photothermal refraction we decompose the total effective cavity length into a "cold cavity" length, L_c, a "slow" cavity length variation due to photothermal expansion, L_s, and a "fast" cavity length variation due to photothermal refraction, L_f, so that,

$$L(t) = L_c(t) + L_s(t) + L_f(t), \tag{5}$$

where the time dependence of L_c is externally controlled, e.g., by the external PZT ramp. Following the approach

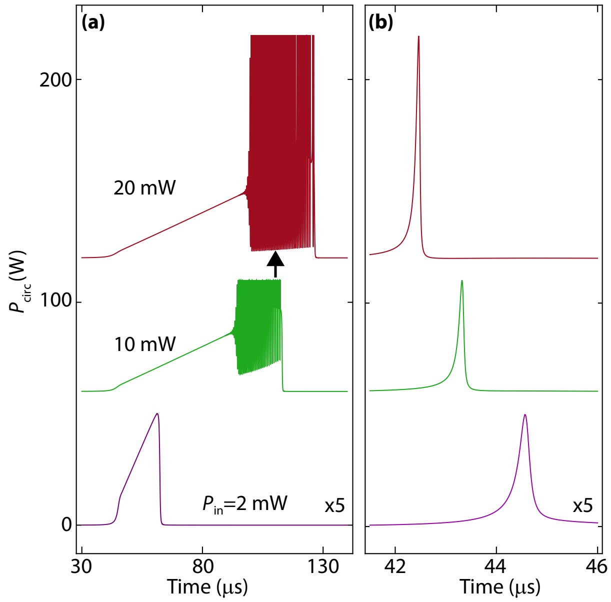

FIG. 4: Circulating power [Eq. (9)] computed numerically from the solution of the differential Eqs. (7) and (8), for three different input laser powers. A PZT scan rate of 8.8 pm/μs as in the data of Fig. 1 was assumed, as well as B_s = 18 pm/W, $B_f = -0.9$ pm/W, $\tau_s = 4$ μs, and $\tau_f = 0.15$ μs. (a) The cavity length is increasing and $L_0 = 400$ pm. (b) The cavity length is decreasing and $L_0 = -400$ pm. Traces are offset vertically by 60 W for clarity.

of Ref. [12] we describe the thermally-driven evolution of L_s and L_f via a linearized power dependence, i.e.,

$$\frac{dL_{s,f}(t)}{dt} = -\frac{1}{\tau_{s,f}}\Big(L_{s,f}(t) + B_{s,f}\alpha P_{\rm in}\mathcal{L}\{L(t) - L_{\rm res}\}\Big), \tag{6}$$

where $L_{\rm res}$ is the cold cavity resonance length. When the cold cavity length is varied at a rate $r_{\rm scan}$ starting at a displacement L_0 from resonance, i.e., $L_c(t) = L_{\rm res} - r_{\rm scan}t + L_0$, the two coupled equations governing the dynamics of the cavity resonance are

$$\dot{L_s} = \frac{-1}{\tau_s}\Big(L_s + B_s\frac{\alpha P_{\rm in}}{1 + (\frac{4\mathcal{F}}{\lambda}(L_s + L_f - r_{\rm scan}t + L_0))^2}\Big) \tag{7}$$

$$\dot{L_f} = \frac{-1}{\tau_f}\Big(L_f + B_f\frac{\alpha P_{\rm in}}{1 + (\frac{4\mathcal{F}}{\lambda}(L_s + L_f - r_{\rm scan}t + L_0))^2}\Big). \tag{8}$$

V. NUMERICAL EVALUATION

We have numerically integrated Eq. (7) and Eq. (8) to obtain the time-dependent quantities $L_s(t)$ and $L_f(t)$. These then provide the time-dependent circulating power, as

$$P_{\rm circ}(t) = \frac{\alpha P_{\rm in}}{1 + (\frac{4\mathcal{F}}{\lambda}(L_s(t) + L_f(t) - r_{\rm scan}t + L_0))^2}, \tag{9}$$

plotted in Fig. 4 for several input powers. This quantity is directly proportional to the experimentally measured cavity transmission. The scan rate set in the simulation was identical to that in the experiment, i.e., $|r_{\rm scan}|$ = 8.8 pm/μs. The "thermal gain" coefficients B_s = 18 pm/W, $B_f = -0.9$ pm/W, and the "thermal loss" coefficients $\tau_s = 4$ μs, and $\tau_f = 0.15$ μs, were chosen heuristically as a best match to the experimental data, starting with the independently estimated values for these coefficients (section III C). Fig. 4(a) shows the circulating power during the "up-ramp" (increasing cavity length and L_0 = 400 pm) while Fig. 4(b) shows the circulating power during the "down-ramp" (decreasing cavity length and $L_0 = -400$ pm). A zoomed view into the $P_{\rm in}$ = 20 mW trace of Fig. 4(a) at t = 110 μs (indicated by the arrow) is shown in Fig. 5(a). Vertically aligned in time, Fig. 5(b), Fig. 5(c), Fig. 5(d) show the corresponding simulated cavity length change associated with photothermal expansion, the cavity length change associated with photothermal refraction, and their sum, respectively. The latter reveals how the overall cyclical variations in effective total cavity length originate in partially compensating expansion/refraction induced variations.

VI. DISCUSSION

It is clear from Fig. 4 and Fig. 5 that Eqs. (7) and (8), despite their simplicity, simulate well the experimental observations of Fig. 1 and Fig. 2. The evolution into "triangular" lineshapes at moderate input power can be captured, and the emergence of the periodic spiking at high input powers is reproduced. Such self-sustained oscillations are encountered in many other physical systems, for example neural cells [28]. In optical systems, self-sustained oscillations and excitability were previously found in both passive macroscopic optical resonators [12, 13], as well as in resonators incorporating a gain medium [29–33]. The commonality, which has its mathematical origin in a system of coupled ordinary differential equations, is the emergence of periodic orbits via a "Hopf bifurcation," similar to those which arise in the van der Pol [34] and FitzHugh-Nagumo [35] problems.

The nonlinear dynamics of semiconductor lasers are typically investigated by observing the light output in response to external perturbations in the form of short-pulse stimuli [29–33]. In these systems with an intentionally incorporated nonlinearity, excitable behavior is most often driven by charge carrier density and thermal dynamics. In nominally empty but mechanically compliant macroscopic high finesse resonators, excitability has been studied in detail both theoretically and experimentally with radiation pressure as one of the driving forces [12, 13]. In the present work using microscopic high finesse resonators, we observe self-sustained stable oscillations above a threshold input coupling, despite the fact that the resonator contains no gain material and that

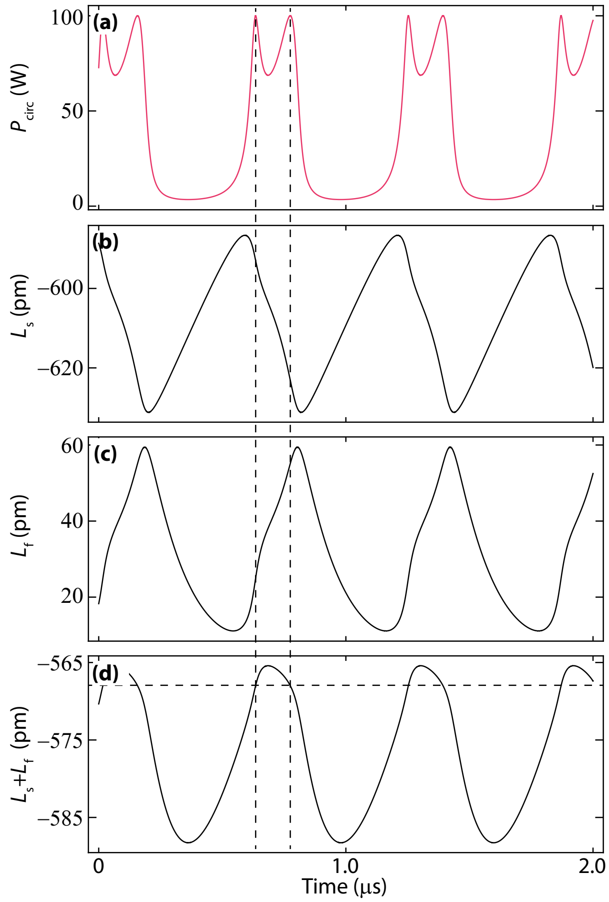

FIG. 5: (a) Zoomed view of the trace at $P_{\rm in}$ = 20 mW relative to time t = 110 μs as indicated by the arrow in Fig. 4(a). (b) Time-dependent cavity length change associated with photothermal expansion. (c) Time-dependent cavity length change associated with photothermal refraction. (d) Time-dependent cavity length change associated with both photothermal expansion and photothermal refraction. The horizontal dashed line indicates the location of the resonance.

its mirrors are mechanically non-compliant. These oscillations are driven entirely by thermal dynamics, the description of which is nonetheless mathematically identical to that of Refs. [12, 13] when the mechanical quality factor is low, i.e., in the overdamped regime.

Although we have presented only the results for a specific optical microcavity, we have made similar observations on other microcavities of the same kind, i.e., the plano-concave type based on bulk substrates. In addition, we have also observed such slow-fast dynamics in differently constructed microcavities, including microcavities in which one mirror is at the tip of a single mode fiber ($\mathcal{F}$=30 000, and $w_0 \approx 2.2$ μm) [9, 15], and a nominally planar cavity built on bulk substrates ($\mathcal{F}$=140 000, and $w_0 \approx 30$ μm). Slow-fast dynamics from photothermal expansion and photothermal refraction is therefore a universal feature expected in any Fabry-Perot optical microcavity. The main difference in dynamics that were found between the different cavity systems investigated are the time scale (period and duration of spikes in particular) which relates to the cavity geometry via the mode spot size. For example, in a cavity built on mirrors with larger radius of curvature, a larger mode spot size implies a longer thermal timescale, and thus less frequent spiking.

The slow-fast dynamics in the experiment and in the theory of Fig. 4 take place once the input power exceeds a threshold. The threshold power, $P_{\rm thresh}$, depends strongly on the cavity finesse which determines the cavity circulating intensity and the cavity displacement sensitivity. For $P_{\rm in} > P_{\rm thresh}$ self-sustained oscillations are observed for certain initial conditions. In particular, for a given input laser frequency, the initial cavity length must to be set such that the system is close to and on the "short" side of the resonance. Experimentally, such initial conditions are adjusted piezoelectrically. Ideally, the piezoelectric adjustment would make it possible to create any initial detuning with arbitrary precision before light is introduced into the cavity. In practice, however, the precision and repeatability of the cavity length adjustment is limited due to the adjustment mechanism itself, for example due to piezo creep, but also because of the extreme sensitivity of high-finesse resonators to external perturbations. For these reasons, the comparison between experiment and theory presented here was done while scanning the cavity length, which offers a more precise approach. Due to the fact that the scan rate is slow compared to the self-sustained thermomechanical oscillations, no loss of generality is incurred. Nevertheless, it is also possible to *approximately* set the initial cavity length, either manually or by interrupting the scan. This is illustrated in Fig. 6 for two initial settings. Under these conditions, the resulting oscillations can persist until unavoidable external perturbations such as laboratory temperature fluctuations and acoustic disturbances cause a significant enough cavity resonance shift to leave the stable oscillatory regime. We have experimentally observed at a minimum millions of uninterrupted cycles which is remarkable given that the cavity resonance linewidth is at the picometer length scale. To illustrate this stability, we have computed numerical derivatives of experimental data and constructed the "phase space" plots shown in Fig. 6.

Physically, according to our model, the dynamics seen here should be viewed as fast mechanical bulging, i.e., swelling and de-swelling, of the mirror surface due to thermal expansion accompanied by periodic refractive index variations. They obviously constitute a substantial deviation from normal desired operation of a microcavity. In particular the fast local temperature variations introduced by this process, and possible secondary effects derived therefrom, such as the generation of thermoelastic waves [23, 36], could affect quantum optical applications such as chemical sensing [9]. For example, the thermoelastic waves may generate a power-dependent background signal associated with Raman scattering in

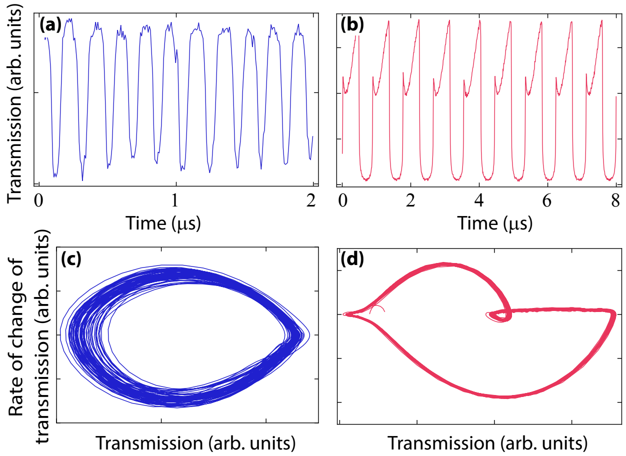

FIG. 6: (a) Experimental cavity transmission as a function of time for an initial displacement from resonance of approximately one half linewidth, for $P_{\mathrm{in}} = 10$ mW (the cavity length is *not* scanned). (b) Same as in (a) but for an initial displacement from resonance of approximately 1/10 of a linewidth. (c) Phase space plot (time derivative of cavity transmission vs. cavity transmission) for the same conditions as in (a) but based on data covering a total time of 10 µs. (d) Phase space plot for the same conditions as in (b) but based on data covering a total time of 40 µs.

the coating [36]. We also note that we have observed irreversible reductions in cavity finesse when operating at input powers above 40 mW in this highly oscillatory regime.

Our analysis shows that the dynamics reported here have their roots in small residual absorption in the dielectric mirror coatings. Despite the interesting physical aspects of these dynamics, they can ultimately be an impediment to the use of high-finesse optical microcavities for any process benefiting from increased circulating intensity localized to a small microscopic volume. However, since ultralow loss coatings with absorption significantly below the absorption seen in the present mirrors have already been fabricated [11], it is likely that microcavities of the same dimension as those investigated here can be manufactured which may sustain average circulating intensity significantly exceeding 1 GW/cm^2 without inducing any slow-fast dynamics due to the competition of photothermal expansion and photothermal refraction. Nonetheless, with an increased cavity finesse and circulating power, it is possible that slow-fast dynamics due to the competition of photothermal expansion and radiation pressure will take place instead [12, 13], even in bulk rigid structures not intended to resonate on any specific mechanical mode. For both cases, it is conceivable that the slow-fast dynamics can be put to use in applications such as waveform generation or as a displacement/temperature sensing technique.

VII. CONCLUSIONS

To summarize, we have investigated with high temporal resolution the transmission of a microcavity of high finesse (60 000) and small mode volume (mirror separation of only few microns) under relatively large input and thus circulating powers (circulating intensity as high as about 700 MW/cm^2). Strong deviations from Lorentzian lineshapes and from triangular bistability lineshapes have been observed. In particular, the emergence of oscillations at >1 MHz frequency are seen for input powers in excess of several mW. Based on a theoretical analysis we ascribe these oscillations to slow-fast dynamics due to the competition between photothermal expansion and photothermal refraction, induced by light absorption in the coating. We speculate that with improved coatings of lower light absorption a further increase in circulating intensity will eventually lead to slow-fast dynamics involving the radiation pressure force, even in cavities made on bulk substrates. Such dynamics may be interesting in their own right for example for use in bulk acoustic cavity optomechanics.

Acknowledgments

The authors acknowledge financial support from the Defense Threat Reduction Agency under HDTRA12-1-0040, and from the Florida High Tech I-4 Corridor Matching Grants program.

[1] K. J. Vahala, Nature **424**, 839 (2003).
[2] T. J. Kippenberg, H. Rokhsari, T. Carmon, A. Scherer, and K. J. Vahala, Phys. Rev. Lett. **95**, 033901 (2005).
[3] J. D. Thompson, B. M. Zwickl, A. M. Jayich, F. Marquardt, S. M. Girvin, and J. G. E. Harris, Nature **452**, 72 (2008).
[4] J. Chan, T. P. Mayer Alegre, A. H. Safavi-Naeini, J. T. Hill, A. Krause, S. Gröblacher, M. Aspelmeyer, and O. Painter, Nature **478**, 89 (2011).
[5] B. P. Abbott *et al.* (LIGO Scientific Collaboration and Virgo Collaboration), Phys. Rev. Lett. **116**, 061102 (2016).
[6] Y. Colombe, T. Steinmetz, G. Dubois, F. Linke, D. Hunger, and J. Reichel, Nature **450**, 272 (2007).
[7] C. J. Hood, T. W. Lynn, A. C. Doherty, A. S. Parkins, and H. J. Kimble, Science **287**, 1447 (2000).
[8] R. Salter, J. Chu and M. Hippler, Analyst. **137**, 4669 (2012).
[9] B. Petrak, N. Djeu, and A. Muller, Phys. Rev. A **89**, 023811 (2014).
[10] T. Carmon, L. Yang, and K. J. Vahala, Opt. Express **12**, 4742 (2004).
[11] K. An, B. A. Sones, C. Fang-Yen, R. R. Dasari, and M. S. Feld, Opt. Lett. **22**, 1433 (1997).

[12] F. Marino, M. De Rosa, and F. Marin, Phys. Rev. E **73**, 026217 (2006).
[13] F. Marino and F. Marin, Phys. Rev. E **87**, 052906 (2013).
[14] B. Petrak, K. Konthasinghe, S. Perez, A. Muller, Rev. Sci. Instrum. **82**, 123112 (2011).
[15] D. Hunger, T. Steinmetz, Y. Colombe, C. Deutsch, T. W. Hänsch and J. Reichel, New J. Phys. **12**, 065038 (2010).
[16] D. Hunger, C. Deutsch, R. J. Barbour, R. J. Warburton and J. Reichel, AIP Advances **2**, 012119 (2012).
[17] J. Gallego, S. Ghosh, S. K. Alavi, W. Alt, M. Martinez-Dorantes, D. Meschede, L. Ratschbacher, Appl. Phys. B **122**, (2016).
[18] F. Monifi, J. Zhang, S. K. Özdemir, B. Peng, Y. Liu, F. Bo, F. Nori, and L. Yang, Nat. Photon. **10**, 399 (2016).
[19] H. Kogelnik and T. Li, Appl. Optics **5**, 1550 (1966).
[20] H. Rokhsari and K. J. Vahala, Opt. Lett. **30**, 427 (2004).
[21] E. L. Buckland and R. W. Boyd, Opt. Lett. **21**, 1117 (1996).
[22] P. F. Cohadon, A. Heidmann, and M. Pinard, Phys. Rev. Lett. **83**, 3174 (1999).
[23] T. Požar and J. Možina, Phys. Rev. Lett. **111**, 185501 (2013).
[24] J. F. S. Brachmann, H. Kaupp, T. W. Hänsch, and D. Hunger, Opt. Express **24**, 21205 (2016).
[25] V. B. Braginsky and A.A. Samoilenko, Phys. Lett. A **315** 175 (2003).
[26] D. B. Leviton and B. J. Frey, Proc. SPIE **6273**, 62732K (2006).
[27] A. K. Chu, H. C. Lin, and W. H. Cheng, J. Elect. Mat. **26**, 889 (1997).
[28] E. M. Izhikevich, Int. J. Bifurcation Chaos Appl. Sci. Eng. **10**, 1171 (2000).
[29] M. Giudici, C. Green, G. Giacomelli, U. Nespolo, and J. R. Tredicce, Phys. Rev. E **55**, 6414 (1997).
[30] M. A. Larotonda, A. Hnilo, J. M. Mendez, and A. M. Yacomotti, Phys. Rev. A **65**, 033812 (2002).
[31] S. Barland, O. Piro, M. Giudici, J. R. Tredicce, and S. Balle, Phys. Rev. E **68**, 036209 (2003).
[32] F. Marino, G. Catalan, P. Sanchez, S. Balle, and O. Piro, Phys. Rev. Lett. **92**, 073901 (2004).
[33] A. M. Yacomotti, P. Monnier, F. Raineri, B. B. Bakir, C. Seassal, R. Raj, and J. A. Levenson, Phys. Rev. Lett. **97**, 143904 (2006).
[34] B. van der Pol, Philos. Mag. **3**, 65 (1927).
[35] R.A. FitzHugh, Biophys. J. **1**, 445 (1961); J.S. Nagumo, S. Arimoto, and S. Yoshizawa, Proc. IREE Austr. **50**, 2061 (1962).
[36] B. Petrak, J. Cooper, K. Konthasinghe, M. Peiris, N. Djeu, A. J. Hopkins, and A. Muller, Appl. Phys. Lett. **108**, 091107 (2016).